IEEE Access
Multidisciplinary | Rapid Review | Open Access Journal

Received October 16, 2020, accepted October 30, 2020, date of publication November 5, 2020, date of current version November 18, 2020.

Digital Object Identifier 10.1109/ACCESS.2020.3036189

Tri-State Nanoelectromechanical Memory Switches for the Implementation of a High-Impedance State

GWANGRYEOL BAEK, (Graduate Student Member, IEEE), JISOO YOON, AND WOO YOUNG CHOI, (Senior Member, IEEE)
Department of Electronic Engineering, Sogang University, Seoul 04107, South Korea

Corresponding author: Woo Young Choi (wchoi@sogang.ac.kr)

This work was supported in part by the National Research Foundation (NRF), South Korea, funded by Ministry of Science and ICT (MSIT) through the Intelligent Semiconductor Technology Development Program under Grant NRF-2019M3F3A1A02072089, through the Mid-Career Researcher Program Grant NRF-2018R1A2A2A05019651, and through the Nano-Material Technology Development Program Grant NRF-2016M3A7B4909668, in part by Institute for Information & Communications Technology Planning & Evaluation (IITP) funded by MSIT through the Information Technology Research Center Program under Grant IITP-2020-2018-0-01421, and in part by the Ministry of Trade, Industry and Energy (MOTIE)/Korea Semiconductor Research Consortium (KSRC) through the Technology Innovation Program under Grant 10080575.

ABSTRACT Tri-state nanoelectromechanical (NEM) memory switches are proposed for the implementation of high-impedance state 0 in addition to low-impedance states 1 and 2 for the improvement of conventional complementary metal-oxide-semiconductor-NEM (CMOS-NEM) reconfigurable logic (RL) operations. Although it is well known that the high impedance state of routing switches is essential to prevent the unnecessary data throughput of RL circuits, previously proposed NEM memory switches have only implemented binary states: states 1 and 2. On the contrary, our proposed NEM memory switches can have tri-states, which are achieved by modifying their operation methods and design guidelines.

INDEX TERMS High impedance, nanoelectromechanical (NEM) memory switch, reconfigurable logic (RL), tri-state operation.

I. INTRODUCTION

Reconfigurable logic (RL) operations have been considered to be indispensable for the following applications: deep learning, database searching, system control, and image processing. A common example is a field programmable gate array. On the contrary, owing to both logic and routing parts that comprise complementary metal-oxide-semiconductor (CMOS) devices, conventional CMOS-only RL circuits have limitations such as poor chip density, low performance, and high power consumption [1]. To overcome these limitations, the routing parts are replaced by nanoelectromechanical (NEM) memory switches that are vertically integrated into the CMOS logic parts [2]–[4]. Both experimental and simulation results have proved that monolithic three-dimensional (M3D) CMOS-NEM RL circuits fully adhere to the CMOS-compatible process and achieve a high chip density, high performance, and low power consumption [4]–[9]. However, for the commercialization of M3D CMOS-NEM RL circuits, further research is necessary.

This study addresses some of the challenges faced by M3D CMOS-NEM RL circuits by contributing toward the implementation of a high-impedance state in NEM memory routing switches for efficient routing. The high-impedance state of routing switches is necessary to prevent unnecessary data throughput [10]. For example, if the high impedance state is not provided, data signal paths remain connected even when they do not need to affect the subsequent logic parts. Moreover, if two different data signals are applied to the same node, an undesirable signal distortion may occur. In the case of conventional CMOS-only RL circuits, high impedance states can be easily obtained using tri-state buffers as the routing switches, as shown in Fig. 1(a) [1]. On the contrary, the previously proposed NEM memory routing switches had only binary states with a low impedance: states 1 and 2 [11]; Fig. 1(b) shows their operating mechanism. The pristine state, which is also known as state 0 with high impedance, is only obtainable after fabrication. Once the NEM memory routing switches are operational, they toggle

The associate editor coordinating the review of this manuscript and approving it for publication was Cristian Zambelli.

between the two selection lines ($L1$ and $L2$). The operation is called the switching operation, providing only two low impedance states. This implies that only binary states such as states 1 and 2 are allowed because NEM memory switches are operated in a near-vacuum environment where damping is negligible [7], [12], [13]. Even if switching operation is also dependent on the ratio of adhesion force and restoring force, the pull-in instability, the switch geometry and so on, this manuscript focuses on the ambient pressure issue. Meanwhile, if damping is maintained at a reasonable level, the acceleration of the movable beam will be alleviated, which maintains it between $L1$ and $L2$ without being attached to any of them. On the basis of this theoretical background, tri-state NEM memory switches are proposed in which state 0 with a high impedance as well as states 1 and 2 are restored during operation as shown in Fig. 1(c). For the implementation of the high-impedance state 0, it is critical to toggle the movable beam from either states 1 or 2 into state 0, which is known as the release operation.

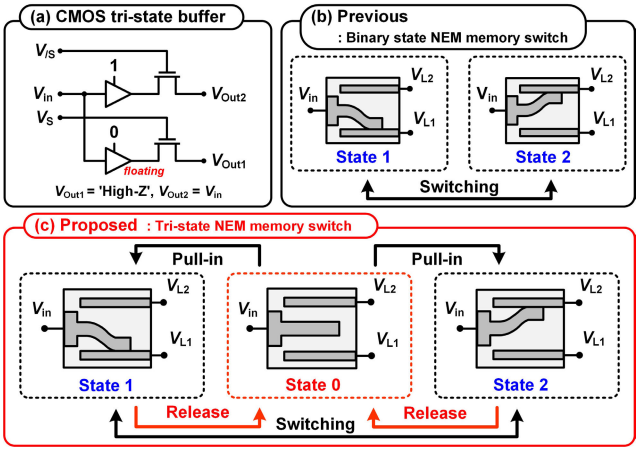

FIGURE 1. (a) CMOS-only tri-state buffer. High impedance state is conducted by disabling the enable signal. (b) Previously-proposed binary state NEM memory switch operation. (c) Proposed tri-state NEM memory switch operation. In State 0, neither of the selection lines are connected to the movable beam. Toggling from (State 0) to (State 1 or 2), toggling from (State 1 or 2) to (State 0), and toggling between State 1 and 2 are called pull-in, release, and switching operation, respectively.

The proposed tri-state NEM memory switches are analogous to binary-state NEM memory switches as presented in [11]–[14]. The three terminal structure is maintained considering the size and fabrication of NEM memory switches. The main difference is the release operation, which is carried out to restore state 0 during operation. Fig. 2(a) shows the conceptual view of our proposed M3D CMOS-NEM RL circuit. The NEM memory switches, comprising a movable beam and two selection lines, are located at the backend copper (Cu) interconnection layers by using dual damascene process as shown in Fig. 2(b). When a voltage is applied between the movable beam and the two selection lines, the beam moves between $L1$ and $L2$ owing to the electrostatic force. The beam is then attached to one of the selection lines (states 1 and 2) or remains in the middle without contacting

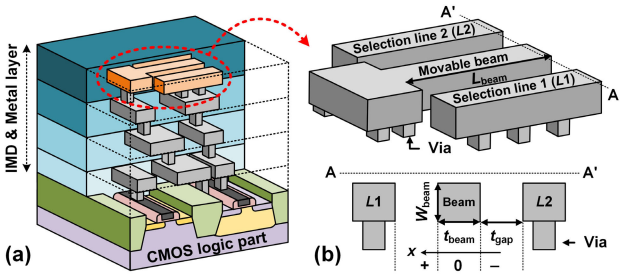

FIGURE 2. (a) Schematic view of a M3D CMOS-NEM RL circuit. (b) Enlarged view of a NEM memory switch. x means beam tip displacement.

the selection lines (state 0). This study focuses on the design guidelines of the release operation to implement tri-state NEM memory switches.

II. SIMULATION ENVIRONMENTS

Henceforth, the release operation will be discussed based on the one-dimensional analytical parallel plate model and the 3D finite-element analysis (FEA). Fig. 3 shows the equivalent circuits of NEM memory switches for states 0, 1, and 2. The value of contact resistance (R_{co}) is shown in Table 1 assuming that 15 % of the movable beam is in contact with the selection lines [15], [16]. In the case of the analytical model, the following d'Alembert's equation is calculated to obtain the beam tip displacement (x) as defined in Fig. 2(b) [17].

$$m_e \frac{d^2x}{dt^2} + b\frac{dx}{dt} + kx = F_{elec} + F_{ad} \tag{1}$$

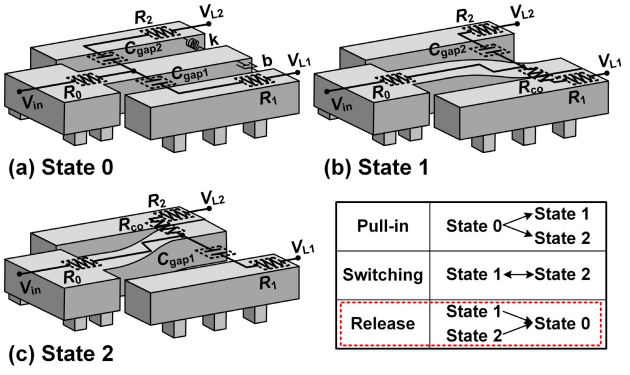

FIGURE 3. Equivalent circuit of NEM memory switches (a) in State 0 (b) in State 1 (c) State 2 and their operations.

where m_e represents the effective beam mass, which is 0.4x the actual beam mass, b denotes the damping coefficient, and k denotes the beam spring constant. b and k are calculated as follows [18]:

$$b = \frac{3\beta\mu_{eff}L_{beam}W_{beam}}{2\pi t_{gap}^3} \tag{2}$$

$$k = \frac{2EW_{beam}t_{beam}^3}{3L_{beam}^3} \tag{3}$$

TABLE 1. Design parameters of NEM memory switches.

Parameters	Values
Technology node	65 nm
CMOS supply voltage (V_{DD})	1.2 V
Switching voltage (V_s)	0.96 V
Beam length (L_{beam})	4.5 μm
Beam width (W_{beam})	126 nm
Beam thickness (t_{beam})	70 nm
Initial gap (t_{gap})	70 nm
Beam material	Cu
Young's modulus (E)	110 Gpa
Dielectric constant of vacuum (ε_0)	8.85 pF/m
Damping fitting parameter (β)	0.15
Surface adhesion force per unit area (p)	4.5 nN/μm^2
Van der Waals distance (d_{vdw})	1.5 nm [21]
Contact resistance (R_{co})	5.7 kΩ

where μ_{eff} means the effective viscosity [19]. In (1), kx and bdx/dt correspond to the spring force (F_r) and damping force (F_{damp}), respectively. β is a fitting parameter for F_{damp}. In addition, the electrostatic force (F_{elec}) and adhesion force (F_{ad}) are derived as [11]

$$F_{elec} = \begin{cases} \dfrac{\varepsilon_0 L_{beam} W_{beam}(V_{L1} - V_{in})^2}{2(t_{gap} - x)^2} & \text{when } V_{L2} - V_{in} = 0\text{V} \\ \dfrac{\varepsilon_0 L_{beam} W_{beam}(V_{L2} - V_{in})^2}{2(t_{gap} + x)^2} & \text{when } V_{L1} - V_{in} = 0\text{V} \end{cases} \tag{4}$$

$$F_{ad} = \begin{cases} pL_{beam} W_{beam}(d_{vdw} - (t_{gap} - x))/d_{vdw} \\ \qquad \text{when} t_{gap} - d_{vdw} \le |x| \le t_{gap} \\ 0 \qquad \text{when } 0 \le |x| \le t_{gap} - d_{vdw} \end{cases} \tag{5}$$

Because NEM memory switches are fabricated during CMOS backend process, the influence of moisture on F_{ad} will be ignored in this work. Other design parameters are summarized in Table 1. Considering the CMOS-compatible process, the beam width (W_{beam}) and thickness (t_{beam}) refer to the 65-nm node of International Technology Roadmap for Semiconductors memory switches that operate under the supply voltage (V_{DD}) of CMOS baseline circuits [20]. For the operation margin, the switching voltage (V_s) is set at 0.8x supply V_{DD} of CMOS baseline logic circuits. β is fixed at 0.15 in the analytical model. F_{damp} issues will be discussed in detail in the following section. Fig. 4 shows the 3D FEA model of our proposed NEM memory switch which is simulated using a commercial tool [22].

The aforementioned two models are applied to emulate the release operation. The analytical model provides physical insights while the FEA model calculates more accurate results, reflecting the actual shape of the NEM memory switches. Our FEA model, however, has a limitation: F_{ad} is assumed to be constant within a certain range rather than gradually increasing as the movable beam approaches the selection lines; thus, the FEA results regarding the release operation will be discussed while considering the analytical results.

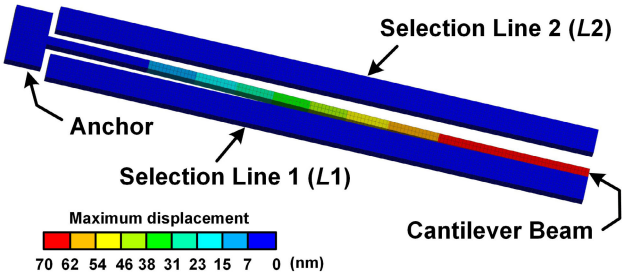

FIGURE 4. 3D FEA model of a NEM memory switch.

III. RESULTS AND DISCUSSION

To implement the tri-state NEM memory switches, state 0 should be restored from states 1 and 2. In states 1 and 2, the NEM memory switches maintain a signal path in a non-volatile manner because F_{ad} is designed to be greater than F_r. For a simple discussion, it is assumed that state 1 is toggled into state 0. When the voltage applied to $L2$ (V_{L2}) turns positive, the beam leaves $L1$. Then, F_r as well as F_{elec} accelerate the beam towards $L2$, which makes state 0 hard to restore. Thus, it is necessary to suppress the beam acceleration during the release operation for the implementation of state 0.

For this purpose, two ideas are proposed in this article. First, the ambient pressure of NEM memory switches should be increased. Conventionally, NEM memory switches have been assumed to operate under the near-vacuum condition. In this case, b is negligible for F_{damp} and can be neglected during the movement of the beam. Consequently, once the beam leaves $L1$, it easily gets attached to $L2$. However, as the ambient pressure increases, F_{damp} also increases, thereby decelerating the beam. Thus, the beam's motion towards $L2$ is hindered by F_{damp}. A higher pressure increases μ_{eff} [19] because the mean free path is inversely proportional to the ambient pressure [23]. Considering (1) and (2), beam acceleration is suppressed as the ambient pressure increases. Second, pulsed V_{L2} is preferred to the constant V_{L2}. For this purpose, the pulse width (T) and amplitude (V) of V_{L2} should correspond to the time required to pull the beam off from the selection lines. Combining both the ideas enables the release operation. As soon as the beam leaves $L1$, it moves only because of its own elastic potential energy. The beam motion is continuously hindered by F_{damp} until the beam loses its energy to reach $L2$, which implies state 0 is restored from state 1.

Fig. 5 shows the relation between forces of the analytical model in the switching and release operation. Net force (F_{net}) is calculated as $F_{elec} + F_{ad} - F_r - F_{damp}$. As F_r is linearly proportional to x, the curve shape of F_r is analogous to that of x. In the early stages of the switching and release operation, the NEM memory switch is in state 1 in a nonvolatile manner,

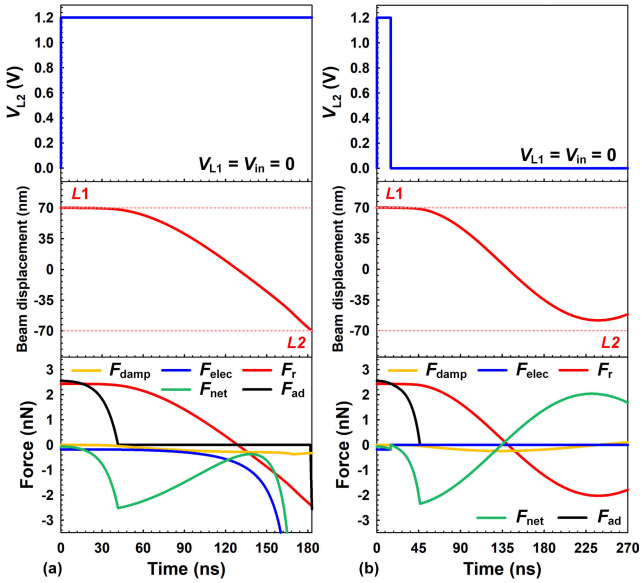

FIGURE 5. V_{L2}, beam displacement, and forces as a function of time calculated by the analytical model during (a) switching and (b) release operation. F_{net} is calculated as $F_{elec} + F_{ad} - F_r - F_{damp}$.

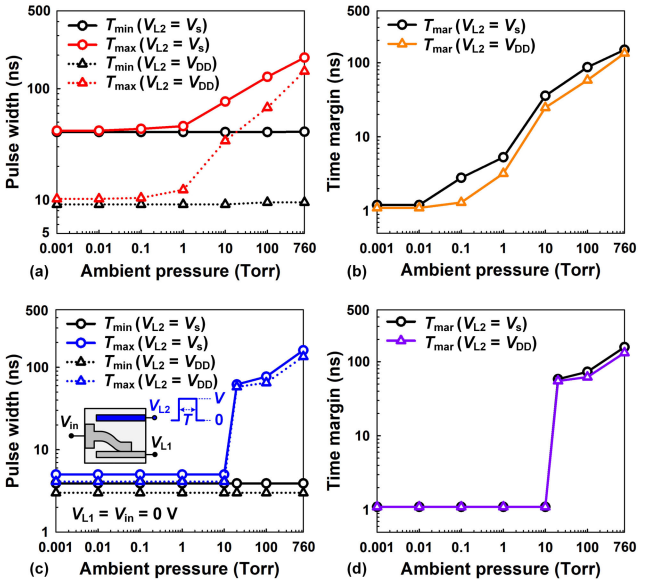

FIGURE 6. (a) T_{min}, T_{max}, and (b) T_{mar} required for tri-state operation as a function of ambient pressure calculated by the analytical model. (c) T_{min}, T_{max}, and (d) T_{mar} required for tri-state operation as a function of ambient pressure calculated by the FEA model. Two voltage levels are assumed for V_{L2}: V_s and V_{DD}.

which implies that F_{ad} is greater than F_r. Then, long- and short-pulse V_{L2}s are applied for the switching and release operation, respectively. In the former case, a nonzero V_{L2} is applied continuously until the beam tip is attached to $L2$ as shown in Fig. 5(a). Thereafter, the absolute value of F_{elec} increases exponentially following (4) as x decreases, which implies that the beam is accelerated to $L2$: switching operation. On the contrary, in the latter case, nonzero V_{L2} is applied only until F_r becomes greater than F_{ad} as shown in Fig. 5(b). Once V_{L2} becomes zero, the only force which makes the beam move towards $L2$ is F_r, which is hindered by F_{damp}. As the ambient pressure increases, the beam experiences a greater F_{damp}. The direction of F_{net} is then turned over so that the beam stops in the air gap without reaching either $L1$ or $L2$: the release operation.

Fig. 6 shows the T of V_{L2} for a tri-state operation as a function of the ambient pressure using the analytical and FEA model. T_{min} and T_{max} represent the minimum and maximum T required to obtain state 0. If T becomes shorter than T_{min}, neither release nor switching occur owing to the F_{ad} within the van der Waals distance. On the contrary, if T becomes greater than T_{max}, switching occurs rather than release, which leads to a binary state operation rather than a tri-state one. T_{min} does not significantly vary with the variation of the ambient pressure because it is mainly determined by F_{ad} and van der Waals distance (d_{vdw}). On the contrary, as the ambient pressure increases, T_{max} becomes greater because a high ambient pressure allows a longer T to stop the beam in the middle of the air gap than at a low ambient pressure. To summarize, T should remain between T_{min} and T_{max} to implement state 0. The time margin (T_{mar}) is defined as the difference between T_{max} and T_{min}, which increases as the ambient pressure increases both in the analytical and FEA model as shown in Figs. 6(b) and 6(d). It implies that a low ambient pressure is desirable for the binary state operation while a high ambient pressure is desirable for the tri-state operation in terms of the controllability of T. Additionally, Fig. 6 shows the two cases of different V values: V_s and V_{DD}. On the whole, the V value is not considerably affected by the ambient pressure because the separation of the beam from one of the selection lines is mainly affected by F_{ad} which is independent of the ambient pressure. In the case of the analytical model shown in Fig. 6(a), T_{min}, T_{max}, and T_{mar} at $V = V_s$ are $\sim$ 4.4x, $\sim$ 4.1x, and $\sim$ 0.3x greater than those at $V = V_{DD}$, respectively. According to the FEA model shown in Fig. 6(c), T_{min}, T_{max}, and T_{mar} at $V = V_s$ are $\sim$ 1.3x, $\sim$ 0.2x and $\sim$ 0.2x greater than those at $V = V_{DD}$, respectively. This is because V_s is fixed at 0.8x V_{DD}, as mentioned before. It takes a longer duration to pull the beam off from the selection line and to stop the beam in the air gap, which leads to greater T_{min} and T_{max} values because the F_{elec} applied to the beam is lower when applying V_s than when applying V_{DD}. Owing to the abrupt increase of T_{max} compared with the T_{min} increase, a greater T_{mar} value is obtained, which implies that a lower V_{L2} is more desirable in the implementation of a tri-state operation. Finally, it needs to be mentioned that Fig. 6(c) shows a steep transition of T_{max} between 10 and 100 Torr. It is a result of the limitation of the commercial FEA simulator where a constant F_{ad} is applied within van der Waals distance.

Interestingly, the analytical model overestimates the influence of the ambient pressure compared with the FEA model. As shown in Fig. 6, the analytical model predicts a longer T_{mar} than the FEA model at the same atmospheric pressure.

The influence of the atmospheric pressure and V on $T_{\min}$ is also overestimated because the FEA model reflects the actual shape of the cantilever beam [24]. For example, the analytical model assumes that forces are equally distributed on the entire beam surface. However, the FEA model includes non-uniformly distributed forces due to a one-sided anchor. The beam part near the anchor barely moves compared with the beam tip, which results in a reduced F_{damp}. On the contrary, F_{r} applied near the anchor is greater than that applied near the beam tip because k is inversely proportional to L_{beam}^3. It implies that near the anchor, F_{r} is a dominant factor over F_{damp}. Thus, the time required for the switching operation is overestimated in the case of the analytical model method.

Finally, the release time (T_{r}) will be discussed. T_{r} is defined as the difference between the time when the beam leaves $L1$ and the time when the amplitude of beam tip oscillation becomes less than $t_{\text{gap}} \cdot e^{-1}$ ($\sim$ 25 nm in this work) as shown in Fig. 8. Fig. 7 represents T_{r} with the variation of the ambient pressure, normalized T (T_{norm}), and V of V_{L2}. T_{norm} is defined as:

$$T_{norm} = \frac{T - T_{\min}}{T_{mar}} \tag{6}$$

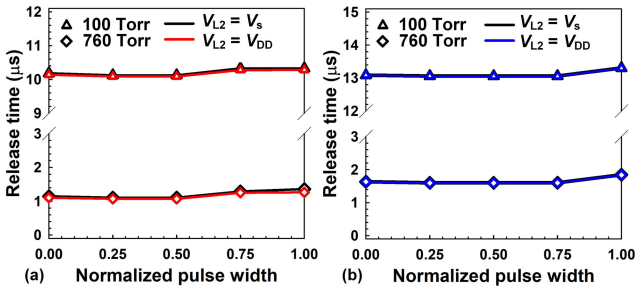

FIGURE 7. Normalized pulse width *vs.* release time calculated by (a) the analytical and (b) FEA model.

In other words, T_{norm} is 0 and 1 when T is equal to $T_{\min}$ and $T_{\max}$, respectively. First, a different T_{norm} *vs.* T_{r} trend is observed near $T_{\text{norm}} = 0.5$, when T_{r} is minimal: the fastest release operation. When T_{norm} is less than 0.5, most of T_{r} is spent on pulling the beam off from the selection line, which is affected by F_{ad}. On the contrary, if T_{norm} is greater than 0.5, more energy is stored in the beam than required for the release operation. The released beam has a high kinetic energy, which requires a longer duration to stop the beam near $x = 0$. Thus, $T_{\text{norm}} = 0.5$ will be optimal when the fastest release operation is obtained with good T margin. Furthermore, as the ambient pressure decreases, T_{r} increases. Lower ambient pressure makes the energy stored in the beam less dissipated by damping. Therefore, it takes a longer duration to suppress the beam from oscillating near $x = 0$. Third, T_{r} is discussed in terms of V. T_{r} at $V = V_{\text{DD}}$ is slightly less than that at $V = V_{\text{s}}$. As a higher V induces greater F_{elec}, the movable beam can be more effectively separated from the selection line. Consequently, it is confirmed that T_{r} is mainly affected by the ambient pressure. The effects of T or V are relatively insignificant even if it becomes stronger as the ambient pressure increases. The fastest release is obtained at $T_{\text{norm}} = 0.5$ and $V = V_{\text{DD}}$.

Fig. 8 shows the release operation under the ambient pressure of 760 Torr predicted by the analytical and FEA model. The T and V of V_{L2} are determined and they satisfy $T_{\text{norm}} = 0.5$ ($T = 75.8$ ns and 69.0 ns for analytical and FEA model, respectively) and V_{DD} conditions. The values of T_{r} are 1.07 and 1.60 μs in the analytical model and FEA model, respectively, which is understood considering that the analytical model overestimates F_{damp}. The T_{r} of tri-state NEM memory switches seems greater than the delay time of conventional CMOS circuits. However, it should be noted that T_{r} only corresponds to the configuration-mode delay, which implies the time to reconfigure circuit topology. Generally, the portion of the configuration mode in the entire operation of RL is very small [3], [11]. Once the circuit topology is determined, NEM memory switches only provide short- or open-circuit condition between CMOS logic parts. Thus, the dynamic-mode delay, which is the time between data signals are transferred from input to output, is similar to the delay time of conventional CMOS circuits [11].

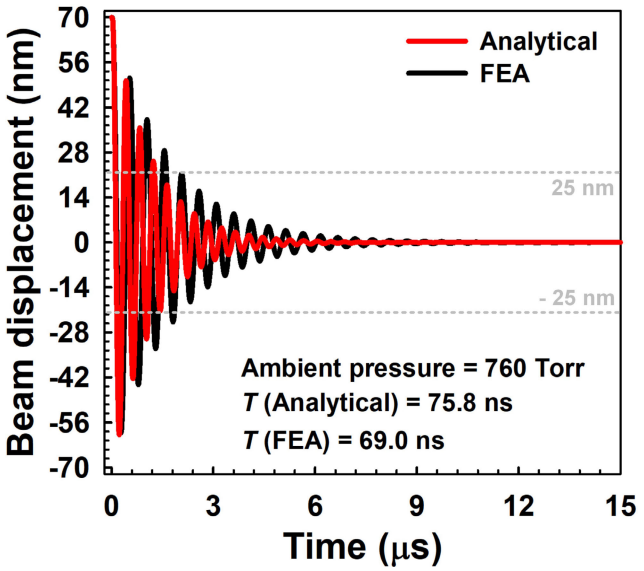

FIGURE 8. Release operation of NEM memory switch under the 760-Torr ambient pressure. The pulse width (T) is set by 75.8 ns for analytical model and 69.0 for and FEA model.

In the actual operation environment of NEM memory switches, F_{ad} at contact area is affected by Joule heating or partial welding. Even if these problems can be mitigated by the cold switching method limiting current density at the contact region [25], F_{ad} may vary whenever switching occurs. To investigate the influence of F_{ad} fluctuation on NEM memory switch operation, Fig. 9(a) shows pulse width *vs.* ambient pressure with the variation of F_{ad}. It is observed that both $T_{\min}$ and $T_{\max}$ increase as F_{ad} becomes larger because more energy is required to separate the movable beam from one of the

selection lines. However, it is observed that T_{mar} is insensitive to F_{ad} as shown in Fig. 9(b). For example, at 760 Torr, T_{mar} varies only ~1.5 % with 10-% increase of F_{ad}. It means that the optimal condition of the original F_{ad} ($T_{norm} = 0.5$) can still be used in spite of F_{ad} variation.

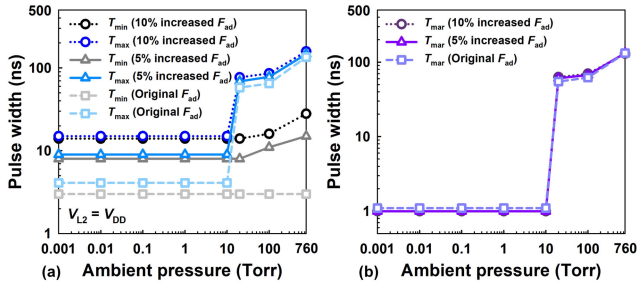

FIGURE 9. FEA-simulated (a) T_{min}, T_{max} and (b) T_{mar} *vs.* ambient pressure with the variation of F_{ad}.

Finally, as the ambient pressure surrounding NEM memory switches increases, the pull-in and switching operation in Fig. 1(c) as well as the release operation are affected. Fig. 10 shows the voltage and time required for the pull-in and switching operation *vs.* the ambient pressure calculated using the FEA model. Fig. 10(a) shows the pull-in operation case. As the ambient pressure increases, the pull-in voltage (V_p) increases owing to an increased F_{damp} that suppresses the beam from reaching the selection lines. However, the influence of the F_{damp} on the pull-in operation is not as strong as that on the release operation because the former shows a slower beam motion. Thus, V_p does not increase until 100 Torr. Same V_p with increased pressure makes T_p slower so that T_p increases ~3% below 10 Torr case. However, V_p increases by ~1% above 10 Torr because F_{damp} starts to affect beam motion. Then, T_p decreases as the ambient pressure becomes higher. Specifically, it shows ~8% faster pull-in operation thanks to increased F_{elec}. Subsequently, in the case of the switching operation shown in Fig. 10(b), it is observed that V_s remains constant and switching time (T_s) increases by ~3 % as the ambient pressure increases from 0.001 to 760 Torr. It is because the beam separation from the selection lines is affected by F_{ad}. Especially, T_s dramatically increases at 760 Torr, because the increasing F_{damp} starts to affect acceleration of the beam. The different aspect with pull-in

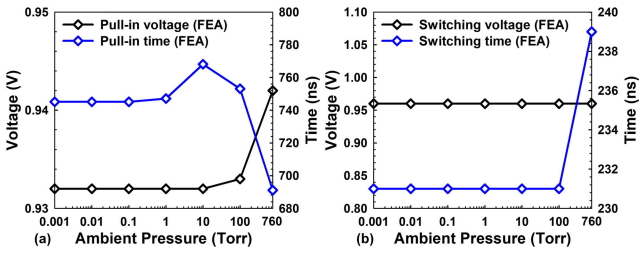

FIGURE 10. Voltage and time required for (a) the pull-in and (b) switching operation with the variation of the ambient pressure.

operation is that switching operation is implemented with the maximum elastic energy. Thus, F_{damp} is less affected by pressure than pull-in operation. Consequently, it is confirmed that only the release operation is sensitive to the ambient pressure unlike the pull-in and switching operation in the case of tri-state NEM memory switches.

So far, the proposed release operation has been discussed based on simulation results. From now, the implementation of the release operation is experimentally verified as shown in Fig. 11. During measurement, compliance current is fixed at 110 nA for cold switching. Initially, the switch is in State 1 as shown in Fig. 11(a). Then, a short pulse whose amplitude and width are 7 V and 400 ns, respectively, is applied to V_{L2}. Finally, the beam is stuck with neither of the selection lines, which means State 0, as shown in Fig. 11(b). Figs. 11(c) and (d) show the current vs. V_{in} curve in each state. In State 1, as shown in Fig. 11(c), the absolute value of I_{in} and I_{L1} is 110 nA while I_{L2} is near zero. This means signal path is formed between the input and $L1$. On the contrary, after the release operation, only leakage level current is observed at all three terminals as shown in Fig. 11(d). It means that the beam is not in contact with either $L1$ or $L2$.

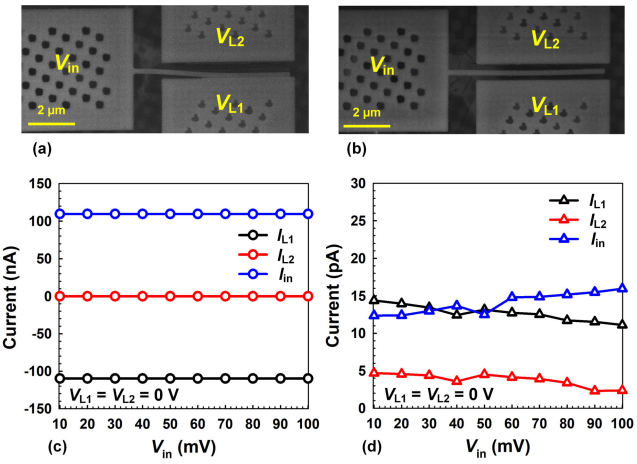

FIGURE 11. Plan view of the fabricated NEM memory switch of (a) State 1 and (b) State 0 by applying pulsed V_{L2}. Measured current *vs.* V_{in} curves in (c) State 1 and (d) State 0.

IV. SUMMARY

Tri-state NEM memory switches and their design guidelines are proposed for the first time to implement state 0 as well as states 1 and 2. By adjusting the ambient pressure and applying a short pulse, NEM memory switches can have three states. It is confirmed that the fastest release operation is conducted at $T_{norm} = 0.5$ and $V = V_{DD}$ under the atmospheric ambient pressure. It is also observed that the pull-in and switching operation is independent of the ambient pressure. The efficient signal routing of CMOS-NEM RL circuits is feasible because state 0, which is uniquely implemented by the release operation, provides the high-impedance state.

REFERENCES

[1] I. Kuon, R. Tessier, and J. Rose, "FPGA architecture: Survey and challenges," *Found. Trends Electron. Des. Autom.*, vol. 2, no. 2, pp. 135–253, 2007, doi: 10.1561/1000000005.
[2] C. Chen, H.-S.-P. Wong, S. Mitra, R. Parsa, N. Patil, S. Chong, K. Akarvardar, J. Provine, D. Lewis, J. Watt, and R. T. Howe, "Efficient FPGAs using nanoelectromechanical relays," in *Proc. 18th Annu. ACM/SIGDA Int. Symp. Field Program. Gate Arrays*, New York, NY, USA, 2010, pp. 273–282, doi: 10.1145/1723112.1723158.
[3] S. Chong, B. Lee, K. B. Parizi, J. Provine, S. Mitra, R. T. Howe, and H.-S.-P. Wong, "Integration of nanoelectromechanical (NEM) relays with silicon CMOS with functional CMOS-NEM circuit," in *IEDM Tech. Dig.*, Washington, DC, USA, Dec. 2011, p. 30, doi: 10.1109/IEDM.2011.6131645.
[4] N. Xu, J. Sun, I.-R. Chen, L. Hutin, Y. Chen, J. Fujiki, C. Qian, and T.-J.-K. Liu, "Hybrid CMOS/BEOL-NEMS technology for ultra-low-power IC applications," in *IEDM Tech. Dig.*, San Francisco, CA, USA, Dec. 2014, p. 28, doi: 10.1109/IEDM.2014.7047130.
[5] A. Peschot, C. Qian, and T.-J. Liu, "Nanoelectromechanical switches for low-power digital computing," *Micromachines*, vol. 6, no. 8, pp. 1046–1065, Aug. 2015, doi: 10.3390/mi6081046.
[6] J. L. Munoz-Gamarra, C. Poulain, W. Ludurczak, S. Hentz, and L. Hutin, "NEMS switches for ultra-low-power digital logic: Challenges and opportunities," in *Proc. IEEE 16th Int. Conf. Nanotechnol. (IEEE-NANO)*, Sendai, Japan, Aug. 2016, pp. 871–874, doi: 10.1109/NANO.2016.7751407.
[7] H. Jo and W. Choi, "Encapsulation of NEM memory switches for Monolithic-Three-Dimensional (M3D) CMOS–NEM hybrid circuits," *Micromachines*, vol. 9, no. 7, p. 317, Jun. 2018, doi: 10.3390/mi9070317.
[8] Q. Luo, Z. Guo, S. Zhang, X. Yang, X. Zou, J. Hong, and L. You, "Crack-based complementary nanoelectromechanical switches for reconfigurable computing," *IEEE Electron Device Lett.*, vol. 41, no. 5, pp. 784–787, May 2020, doi: 10.1109/LED.2020.2983735.
[9] C. L. Ayala, A. Bazigos, D. Grogg, U. Drechsler, and C. Hagleitner, "Experimental demonstration of a nanoelectromechanical switch-based logic library including sequential and combinational gates," in *Proc. 42nd Eur. Solid-State Circuits Conf.*, Lausanne, Switzerland, Sep. 2016, pp. 51–54, doi: 10.1109/ESSCIRC.2016.7598242.
[10] K. Niewiadomski and D. Tutsch, "Low power tristate buffer for mobile applications," in *Proc. 10th Int. Conf. Adapt. Self-Adapt. Syst. Appl.*, Barcelona, Spain, Nov. 2018, pp. 9–14.
[11] Y. Jun Kim and W. Young Choi, "Nonvolatile nanoelectromechanical memory switches for low-power and high-speed field-programmable gate arrays," *IEEE Trans. Electron Devices*, vol. 62, no. 2, pp. 673–679, Feb. 2015, doi: 10.1109/TED.2014.2380992.
[12] W. Y. Choi and H. S. Kwon, "Slingshot pull-in operation for low-voltage nanoelectromechanical memory switches," *IEEE Trans. Electron Devices*, vol. 66, no. 4, pp. 2040–2043, Apr. 2019, doi: 10.1109/TED.2019.2899888.
[13] W. Y. Choi and Y. J. Kim, "Three-dimensional integration of complementary Metal-Oxide-Semiconductor-Nanoelectromechanical hybrid reconfigurable circuits," *IEEE Electron Device Lett.*, vol. 36, no. 9, pp. 887–889, Sep. 2015, doi: 10.1109/LED.2015.2455556.
[14] H. Moon Lee, H. Chan Jo, H. Su Kwon, and W. Young Choi, "Switching voltage analysis of nanoelectromechanical memory switches for monolithic 3-D CMOS-NEM hybrid reconfigurable logic circuits," *IEEE Trans. Electron Devices*, vol. 65, no. 9, pp. 3780–3785, Sep. 2018, doi: 10.1109/TED.2018.2858775.
[15] H. C. Jo, M. H. Kang, and W. Y. Choi, "Selection line optimization of nanoelectromechanical (NEM) memory switches for stress relief," *J. Semicond. Technol. Sci.*, vol. 19, no. 2, pp. 203–207, Apr. 2019, doi: 10.5573/JSTS.2019.19.2.203.
[16] U. Sikder, G. Usai, T.-T. Yen, K. Horace-Herron, L. Hutin, and T.-J.-K. Liu, "Back-End-of-Line Nano-Electro-Mechanical switches for reconfigurable interconnects," *IEEE Electron Device Lett.*, vol. 41, no. 4, pp. 625–628, Apr. 2020, doi: 10.1109/LED.2020.2974473.
[17] G. M. Rebeiz, *RF MEMS: Theory, Design and Technology*. Hoboken, NJ, USA: Wiley, 2003.
[18] W. Weaver, Jr., S. P. Timoshenko, and D. H. Young, *Vibration Problems in Engineering*. Hoboken, NJ, USA: Wiley, 1990.
[19] T. Veijola, H. Kuisma, J. Lahdenperä, and T. Ryhänen, "Equivalent-circuit model of the squeezed gas film in a silicon accelerometer," *Sens. Actuators A, Phys.*, vol. 48, no. 3, pp. 239–248, 1995, doi: 10.1016/0924-4247(95)00995-7.
[20] Semiconductor Industry Association. (2005). *International Technology Roadmap for Semiconductors (ITRS)*. [Online]. Available: http://www.itrs2.net/itrs-reports.html
[21] J. Yaung, L. Hutin, J. Jeon, and T.-J.-K. Liu, "Adhesive force characterization for MEM logic relays with sub-micron contacting regions," *J. Microelectromech. Syst.*, vol. 23, no. 1, pp. 198–203, Feb. 2014, doi: 10.1109/JMEMS.2013.2269995.
[22] *ANSYS Structural Analysis*, ANSYS, Canonsburg, PA, USA, 2009. [Online]. Available: https://www.ansys.com/
[23] G. X. Li and H. G. Hughes, "Review of viscous damping in micromachined structures," in *Proc. Micromachined Devices Compon.*, Aug. 2000, pp. 30–46, doi: 10.1117/12.395618.
[24] S. H. Roh, K. Kim, and W. Y. Choi, "Scaling trend of nanoelectromechanical (NEM) nonvolatile memory cells based on finite element analysis (FEA)," *IEEE Trans. Nanotechnol.*, vol. 10, no. 3, pp. 647–651, May 2011, doi: 10.1109/TNANO.2010.2068056.
[25] V. Pott, H. Kam, R. Nathanael, J. Jeon, E. Alon, and T.-J. King Liu, "Mechanical computing redux: Relays for integrated circuit applications," *Proc. IEEE*, vol. 98, no. 12, pp. 2076–2094, Dec. 2010, doi: 10.1109/JPROC.2010.2063411.

GWANGRYEOL BAEK (Graduate Student Member, IEEE) was born in Daejeon, in 1995. He received the B.S. degree in electronics & electrical engineering from Dankook University, Yongin, South Korea, in 2019. He is currently pursuing the M.S. degree with the Department of Electronic Engineering, Sogang University, Seoul. His current research interest includes nanoelectromechanical (NEM) relays/memory cells.

JISOO YOON was born in Seoul, in 1995. She received the B.S. degree in materials science & engineering from Inha University, Incheon, South Korea, in 2020. She is currently pursuing the M.S. degree with the Department of Electronic Engineering, Sogang University, Seoul. Her current research interest includes nanoelectromechanical (NEM) relays/memory cells.

WOO YOUNG CHOI (Senior Member, IEEE) received the B.S., M.S., and Ph.D. degrees from the School of Electrical Engineering, Seoul National University, Seoul, South Korea, in 2000, 2002, and 2006, respectively. From 2006 to 2008, he held a postdoctoral position with the Department of Electrical Engineering and Computer Sciences, University of California at Berkeley, Berkeley, CA, USA. Since 2008, he has been a Faculty Member with Sogang University, Seoul, where he is currently a Professor with the Department of Electronic Engineering. He has authored or coauthored more than 300 articles in international journals and conference proceedings. He holds more than 50 Korean and U.S. patents. His current research interests include the fabrication, modeling, characterization, and measurement of MOSFETs, and emerging electron devices, and memory.